Electronic Coupling between Heme Electron-Transfer Centers and Its Decay with Distance Depends Strongly on Relative Orientation

Dayle M. A. Smith,*,†,|| Kevin M. Rosso,‡ Michel Dupuis,§ Marat Valiev,|| and T. P. Straatsma⊥

Department of Physics, Whitman College, Walla Walla, Washington 99362, and Environmental Dynamics and Simulation, Chemical Sciences Division, Molecular Interactions and Transformations, Chemical Sciences Division, Molecuar Sciences Software Group, Environmental Molecular Sciences Laboratory, and Computational Biology and Bioinformatics, Computational Sciences and Mathematics Division, Pacific Northwest National Laboratory, Richland, Washington 99352

Received: December 5, 2005; In Final Form: June 13, 2006

A method for calculating the electron-transfer matrix element V_{RP} using density functional theory Kohn−Sham orbitals is presented and applied to heme dimers of varying relative orientation. The electronic coupling decays with increased iron separation according to $V_{RP} = V_{RP}^0 \exp(-\beta r/2)$ with a distance dependence parameter $\beta \approx 2$ Å^{-1} for hemes with parallel porphyrins and either 1.1 or 4.0 Å^{-1} when the porphyrin planes are perpendicular, depending on the alignment of the iron d_π orbital. These findings are used to interpret the observed orientation of the hemes in tetraheme redox proteins such as Flavocytochrome c_3 fumarate reductase (Ifc_3, PDB code 1QJD) of *Shewanella frigidimarina*, another flavocytochrome from the same bacterium (Fcc_3, 1E39) and a small tetraheme cytochrome of *Shewanella oneidensis* strain MR1 (1M1P). Our results show that shifting and rotating the hemes controls the adiabaticity of the three electron hopping steps.

Introduction

Shewanella bacteria are among a class of microbes that are able to use insoluble mineral iron and other metals as final electron acceptors in the respiratory cycle. *Shewanella oneidensis* strain MR1, for instance, is able to reduce soluble, high-oxidation-state metals such as uranium, technetium, and chromium into insoluble low-oxidation-state form and has been studied extensively for use as a bioremediation agent.[1,2] *Shewanella frigidamarina*, as the name implies, was discovered in Antarctic sea ice,[3] and contains several c-type cytochromes, such as flavocytochrome c_3 fumarate reductase (Ifc_3, PDB code 1QJD). Ifc_3 catalyzes the chemical reduction of fumarate to succinate, and its function depends on long-range electron transfer, proton transfer, and conformational transitions in the active site that are controlled by the long-time dynamic behavior of the protein. The Ifc_3 cytochrome transfers electrons, acquired at the cytoplasmic membrane, to the flavin adenine dinucleotide (FAD) active site, via four covalently bound c-type hemes (HEC) in which the iron is ligated by histidine side chains. Figure 1 shows the Ifc_3 protein structure 1QJD, with the hemes, their attached histidines, the FAD active site, and fumarate substrate in detail.

Ifc_3 shares striking similarities with other cytochromes from *S. frigidimarina*, *S. oneidensis*, and many others, particularly with regard to the orientation of the heme planes.[4] Although the functions of these enzymes are different, the roles of the heme groups are the same: transport of electrons over large distances to the active site's cofactor.[4] In all of these tetraheme cytochromes, the porphyrin planes of HEC801 (1QJD residue numbering) and HEC802 are perpendicular to each other and so are the planes of HEC803 and HEC804, whereas HEC802 and HEC803 are stacked and slightly offset. (HEC804 is closest to the active site.)

The present study examines the distance and angular dependence of the orientation of heme dimers on the electron hopping probabilities that govern the mechanism of electron transfer between the hemes in proteins such as Ifc_3. We found that, although the electron-transfer probability between hemes obeys exponentially decaying distance dependence, it also depends strongly on the relative orientation of the heme porphyrin planes. A similar result was observed for $Fe(Cp)_2^{0/+}$ self-exchange.[5]

Computational Methods

Density functional theory (DFT) has been widely used to model the properties of hemes, including the relative energies, high-spin and low-spin states,[6,7] optimized geometries, Mössbauer parameters,[7−13] harmonic frequencies,[7,14,15] and even the electronic structure of an entire cytochrome.[16] The DFT functionals used in these studies included LSDA,[10,11,16] BPW91,[9,12,13,17] and, most commonly, B3LYP.[7,8,12−14,17−19] The electron correlation that is accounted for in DFT makes this level of theory appealing. In many cases, these functionals have provided calculated data in apparent accord with experimental data for many systems and their properties, including for hemes. Our recent study compared optimized geometries, relative spin and oxidation-state energies, and Mössbauer quadrupole splitting parameters for $FeP(Im)_2$ versus $FeP(H_2O)_2$, which has a high-spin ground state.[6] Our study and those of others[17,20] indicate that unrestricted Hartree−Fock (UHF) favors high-spin states, generalized gradient approximation (GGA) functionals favor

* Author to whom correspondence should be addressed. E-mail: smithdm@whitman.edu.

† Department of Physics, Whitman College.

‡ Environmental Dynamics and Simulation, Chemical Sciences Division, Pacific Northwest National Laboratory.

§ Molecular Interactions and Transformations, Chemical Sciences Division, Pacific Northwest National Laboratory.

|| Molecuar Sciences Software Group, Environmental Molecular Sciences Laboratory, Pacific Northwest National Laboratory.

⊥ Computational Biology and Bioinformatics, Computational Sciences and Mathematics Division, Pacific Northwest National Laboratory.

10.1021/jp057068r CCC: $33.50
Published on Web 07/18/2006

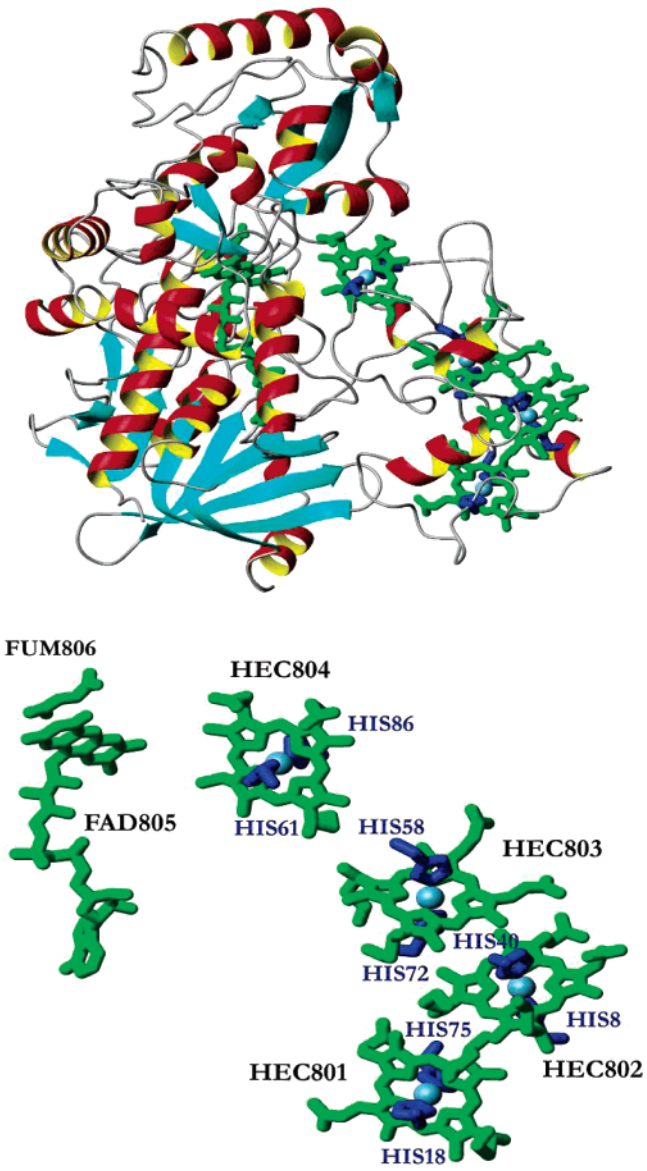

Figure 1. Flavocytochrome c_3 fumarate reductase of *Shewanella frigidimarina* (PDB code 1QJD).

low-spin states, and hybrid functionals that include a fraction of the exact exchange yield small energy differences between low- and high-spin states. B3LYP yielded the best overall correlation with available experimental data and the proper magnitude and sign for the high-spin/low-spin energy difference.[6]

We chose bis(imidazole) iron porphyrin [FeP(Im)$_2$] as a model complex, in which the imidazoles are representative of attached histidine side chains. Our six-coordinate model hemes are oriented, according to the convention, with the iron at the origin and porphyrin nitrogen atoms aligned along the *x*- and *y*-axes (Figure 2).

In most bis(histidine) hemes, the $Fe^{III}(3d)$ electron configuration is $d_{xy}^2(d_{xz},d_{yz})^3$. The mixed $(d_{xz},d_{yz}) = d_\pi$ orbital has been observed in the porphyrin $\pi \leftrightarrow d_\pi$ charge-transfer bands of low-spin ferric hemes such as cytochrome c[21] and high-spin ferrous heme proteins.[22] Several electron paramagnetic resonance (EPR) and NMR experiments of cytochromes and model hemes have shown that low-spin iron(III) porphyrinates have a $d_{xy}^2(d_{xz},d_{yz})^3$ ground state, and now this is widely accepted.[23]

Although high-spin hemes have been observed in equilibrium with low-spin hemes (2% high spin[24]), our recent investigations

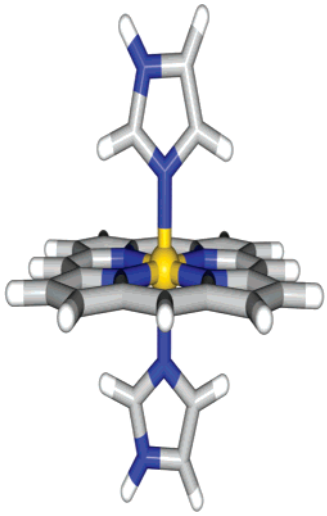

Figure 2. FeP(Im)$_2$ with parallel imidazoles.

of the electronic and nuclear properties of a model heme complex[7] showed that although the iron−imidazole distance is a key structural parameter characteristic of the preference for a low-spin or high-spin electronic configuration, the difference in the iron−imidazole bond length (0.2 Å) and the energy difference (6.7 kcal/mol for ferrous hemes and 8.4 kcal/mol for ferric hemes) between low-spin and high-spin states was large enough that only low-spin hemes are considered in this study.

For the geometry optimizations and electron-transfer calculations, we used the Ahlrich VTZ basis set for iron and Dunning's DZ+Diffuse basis set for the porphyrin and imidazoles, except on the nitrogens bound to iron because including those diffuse functions created an artificially negative charge on the iron centers (752 basis functions for each heme monomer). The starting guess for the open-shell density of the model heme complexes was generated from B3LYP orbitals of ferric and ferrous iron ions, isolated porphyrin, and imidazole fragments, then geometry optimizations were initiated for the ferric and ferrous low-spin hemes.

To investigate the effects of the histidine plane orientation on the heme electronic structure, we calculated torsion potentials for the rotation of one imidazole, leaving the other one fixed. Using the same basis set as above, we calculated torsion potentials with both rigid and relaxed porphyrin configurations.

In the following description of electron transfer (ET) between any two hemes *i* and *j* let R denote an initial, reactants state $\Psi_R = [\text{heme}_i^{II} \times \text{heme}_j^{III}]$ and P denote a final, products state $\Psi_P = [\text{heme}_i^{III} \times \text{heme}_j^{II}]$, using a notation intended to represent the configuration state functions of the hemes in the pair. We calculated the electronic coupling matrix element (V_{RP}) between states R and P, the activation energy (ΔG^*), and the nuclear reorganization energy (λ), all quantities that enter Marcus' ET rate expression.[25] Note that Ψ_R and Ψ_P are nonorthogonal wave functions so that the calculation of V_{RP} requires a bi-orthogonalization of the molecular orbitals of the two states.

Electron transfer occurs at the crossing point (Q_C) between two parabolic potential energy surfaces as a function of the nuclear coordinates, one representing the ET reactants and the other representing the ET products. The energy required to distort the reactants and polarize the surrounding medium into the configuration of the products, or vice versa, is the reorganization energy. Marcus showed that the activation energy (ΔG^*) is $\lambda/4$ for thermally promoted ET in the absence of a net energy change upon ET (zero driving force).[26] At the crossing point, the probability of electron transfer depends on the

electronic interaction between the reactants and products states, which is contained in the term V_{RP}. If V_{RP} is sufficiently large, then the ET is adiabatic, and the ET probability at the crossing point is nearly 100%, and every impingement on the crossing point is assumed by convention to yield the ET products. If V_{RP} is small, then the nonadiabatic (also called diabatic) case is obtained, the ET probability at the crossing point is less than 100%, and only a fraction of the excitations to the crossing-point configuration will yield the ET products. A useful expression that relates V_{RP} and the potential energy landscape at the crossing point is based on Landau and Zener[27,28] and given by Sutin[29,30] as

$$P_{LZ} = 1 - \exp(-2\pi\gamma) \tag{1}$$

where

$$2\pi\gamma = \frac{V_{RP}^2}{h\nu_n}\sqrt{\frac{\pi^3}{\lambda kT}} \tag{2}$$

where ν_n is a typical nuclear vibrational frequency in heme centers (taken as 10^{13} s^{-1}). In our case, the ET reactions are symmetric, and therefore the slopes of the two potential energy surfaces at the crossing point are the same. The symmetry arises primarily from the fact that the protein matrix is not treated explicitly, and therefore any two heme centers in our calculations possess approximately the same electron affinities.

The overall reaction probability must be based on the additional consideration of multiple passages through Q_C, which includes, for example, the descent of the system back down through Q_C where a finite probability of a hop from one surface to another also exists. The overall reaction probability is referred to as κ and is related to P_{LZ} by[30]

$$\kappa = \frac{2P_{LZ}}{1 + P_{LZ}} \tag{3}$$

This overall probability κ is also known as the transmission coefficient and is used as the preexponential electronic factor in Marcus' ET rate equation based on Eyring's transition state theory.[26]

In molecules with a large number of degrees of freedom, such as hemes, it is difficult to calculate the crossing-point structure. This problem is greatly simplified if we exploit the fact that the reduced and oxidized bis(histidine) hemes are structurally very similar.[7] When the ET reactant and product potential energy curves are well approximated by parabolic functions of Q, as is the case here, for small displacements in Q, a good approximation of the reaction coordinate is given by[27]

$$Q(\xi) = \xi Q_R + (1 - \xi)Q_P \tag{4}$$

Using $1 \leq \xi \leq 0$, Q can smoothly change from $Q_R(\xi = 0)$ to $Q_P(\xi = 1)$, going through $Q_C(\xi = {}^1/_2)$. Since the displacement from reactants to products is small, especially for the hemes with parallel ligands, this is an excellent approximation.

The reorganization energy was taken as the sum of internal and external components.[29] The internal component (λ_I) is the energy to distort bonds in the heme groups to the configuration appropriate for electron transfer. We used Nelsen's four-point method[31−33] to compute λ_I from the DFT total energies. This assumes that the structure of the heme groups are independent of each other,[34] a good assumption in this case because of the large distances separating them in Ifc_3. The external component of the reorganization energy (λ_E) is the energy required to polarize the surrounding protein and solvent medium into the configuration consistent with ET and was estimated using Marcus' continuum model[26]

$$\lambda_E = (\Delta e)^2\left(\frac{1}{2r_1} + \frac{1}{2r_2} - \frac{1}{R}\right)\left(\frac{1}{D_{opt}} - \frac{1}{D_s}\right) \tag{5}$$

where Δe is the charge transferred (one electron in this case), r_1 and r_2 are the cavity radii for the reactants, R is the distance of separation, and D_{opt} and D_s are the optical and static dielectric constants of the medium. A spherical cavity radius of 5 Å for the reactants was used, because the radii of the heme groups measured across the plane of the porphyrin ring (4.5 Å) is close to the distance measured across the imidazoles (5.3 Å). The optical and static dielectric constants for the protein matrix were taken as 2 and 10, respectively.[29] We note that these dielectric constants are approximate due to the heterogeneity of the protein structure.[35]

Five heme dimers with different relative orientations were used to study the rotational dependence of the electron transfer (Figures 3A−3E). In dimer A, the heme porphyrins are stacked to allow for good overlap between the iron and the porphyrin atoms that contribute to the spin density. In dimers B and C, the porphyrins are coplanar, and the imidazoles of the two hemes are either coplanar (dimer B) or parallel (dimer C) to examine whether the imidazole torsion affects the electron transfer. In dimers D and E, the porphyrin planes are perpendicular. Dimer D has the edges of the porphyrin planes aligned, whereas the iron of the second monomer is in the plane of the first monomer's porphyrin in dimer E.

Electron-transfer coupling elements were also calculated for consecutive heme pairs, in which the individual hemes were superimposed onto the hemes of the crystal structure of Ifc_3 (Figure 1). The crossing-point geometries of the heme monomers were calculated using eq 4, and the DFT molecular orbitals converged using B3LYP were initiated from the orbitals from the geometry optimizations. The molecular orbitals of each model heme were rotated from the conventional orientation, at which the geometry optimizations were carried out, to its orientation in the cluster, so as to reduce the amount of time required to converge the molecular orbitals (MOs) of the cluster and also to ensure that the Fe(3d) electronic state would be maintained. The MOs for the ET reactant and product states for the three consecutive heme dimer pairs were then converged from a fragment guess using the rotated heme orbitals. The resulting ET reactant and product orbitals were used to calculate electron-transfer coupling elements for the three heme pairs, in which the dominant ET orbital has mostly $Fe(d_\pi)$ character (Figure 4). The calculation of V_{RP} in our code follows the methodology of Farazdel et al. with the exception of one modification adopted for Kohn−Sham wave functions used as characterization of the quasi-diabatic states Ψ_R and Ψ_P. The Hamiltonians of the Kohn−Sham wave functions are state-dependent, so that the secular equations (eq 6)

$$\begin{vmatrix} H_{RR} - ES_{RR} & H_{RP} - ES_{RP} \\ H_{RP} - ES_{RP} & H_{PP} - ES_{PP} \end{vmatrix} = 0 \tag{6}$$

that define the mixing of the two states and their splitting (eq 7)

$$V_{RP} = (1 - S_{RP}{}^2)^{-1}[H_{RP} - S_{RP}(H_{RR} + H_{PP})/2] \tag{7}$$

at the crossing point are not well defined. When using the Hartree−Fock (HF) method to calculate the quasi-diabatic wave

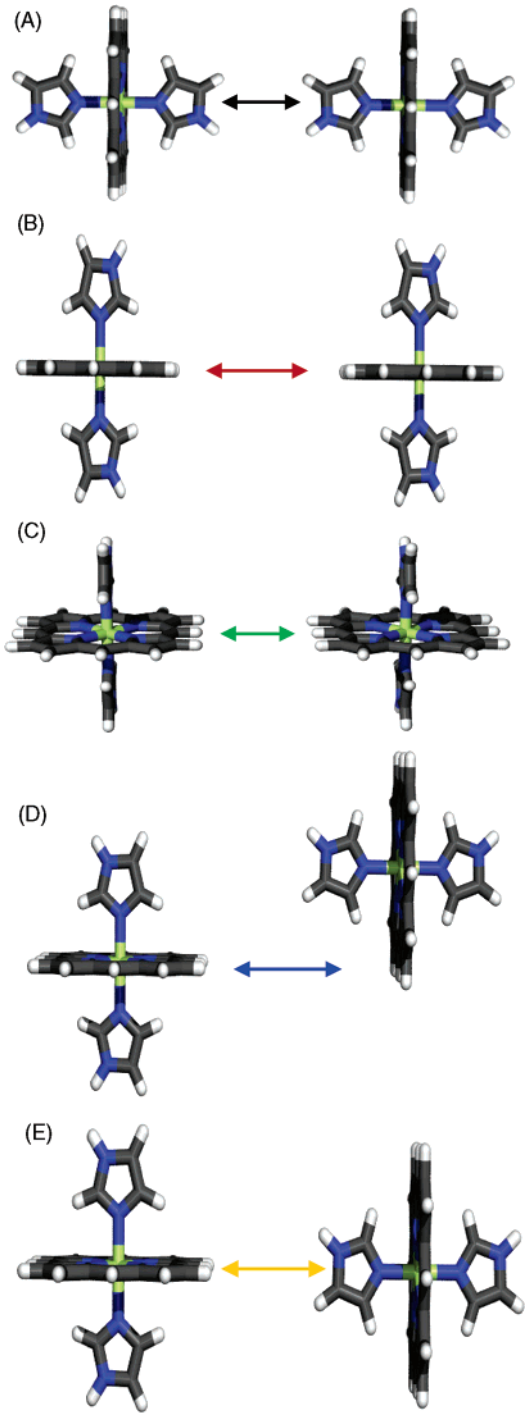

Figure 3. (A) Stacked heme dimer. The exponential dropoff of the electronic coupling with increased separation between the iron centers is $V_{RP} = 1.6 \exp(-1.0r)$, and the ET is fully adiabatic when the separation between iron centers is 11.8 Å^{-1}. (B) Parallel heme dimer with coplanar imidazoles. The exponential dropoff of the electronic coupling with increased separation between the iron centers is $V_{RP} = 8.0 \exp(-1.3r)$, and the ET is fully adiabatic when the separation between iron centers is 13.0 Å^{-1}. (C) Parallel heme dimer with parallel imidazoles. The exponential dropoff of the electronic coupling with increased separation between the iron centers is $V_{RP} = 6.6 \exp(-1.1r)$, and the ET is fully adiabatic when the separation between iron centers is 13.0 Å^{-1}. (D) Perpendicular heme dimer. The exponential dropoff of the electronic coupling with increased separation between the iron centers is $V_{RP} = 540 \exp(-2.0r)$, and the ET is fully adiabatic when the separation between iron centers is 16.3 Å^{-1}. (E) Staggered perpendicular heme dimer. The exponential dropoff of the electronic coupling with increased separation between the iron centers is $V_{RP} = 0.2 \exp(-0.55r)$, and the ET is never fully adiabatic.

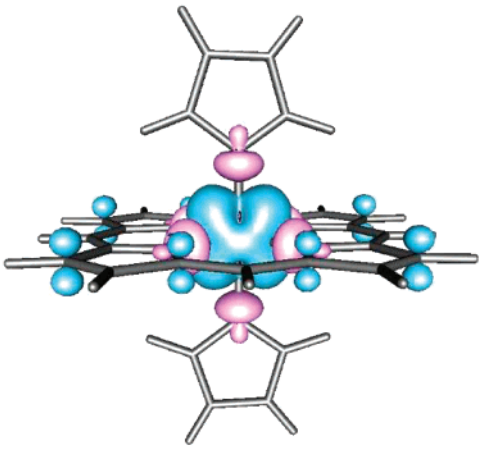

Figure 4. Spin densities for the low-spin ferric model heme. The 0.001 contour level is shown. Blue areas have excess α spin, and pink areas have excess β spin.

functions, the diagonal terms H_{RR} and H_{PP} are taken to be the self-consistent-field HF energies. However, there are no restrictions in the formalism as to where the quasi-diabatic wave functions come from. Therefore, we take the quasi-diabatic wave functions to be the Kohn−Sham determinants with their orbitals that account for electronic correlation, as long as they exhibit the electron-localized character of quasi-diabatic states. In this case the diagonal energy terms H_{RR} and H_{PP} become the electronic energy of the full exact electronic Hamiltonian evaluated with the Kohn−Sham determinants. The data discussed below followed this methodology.

All calculations were performed using the NWChem[36] software package on a Hewlett-Packard supercomputer using up to 256 Itanium-2 processors.

Results and Discussion

Optimized Geometries. We previously reported the geometries of ferric and ferrous hemes with parallel imidazole ligands, with both low-spin and high-spin iron.[7] The most significant differences lie in the iron−imidazole distance, Fe−N$_\epsilon$, and the "core size", which is the average of the four iron−porphyrin nitrogen distances. In the ferrous hemes, the core size is larger than that in the ferric hemes to accommodate the larger ferrous ion. The distances to the axial imidazoles, which, in our model, mimic the histidines of the protein, differ between ferric and ferrous hemes and compared very well with X-ray results.

B3LYP Energies and Electronic Structure. The adiabatic electron affinity (AEA), calculated from the energies of the ferric and ferrous hemes, each at their respective optimized geometries, is 5.17 eV, and the internal reorganization energy (λ_I) is 0.08 eV. Figure 4 shows the spin density of the oxidized model heme. Although the excess α spin density is primarily Fe(d_π), there is also some $\rho^{\alpha-\beta}$ on the porphyrin's carbons and the nitrogens bound to iron.

Imidazole Torsion Potentials. Calculations of the torsional energy profile with respect to imidazole planes orientation show local minima at 0° (cis), 90°, and 180° (trans) configurations (Figure 5). These are the configurations also observed in the protein (1QJD). Yet, our numbers indicate that the heme group itself shows little resistance toward this rotation. Therefore, it is the protein environment that is responsible for persistent orientation of the histidine planes observed in X-ray structure.

Electron Transfer between Model Hemes. Table 1 lists the exponential decay functions describing the distance dependence of the electron-transfer matrix elements for the five model heme

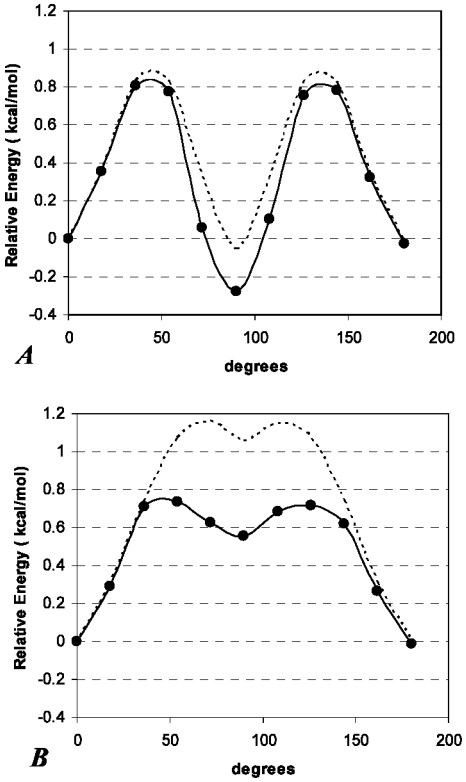

Figure 5. Torsion potentials for (A) reduced and (B) oxidized hemes. Dashed and solid lines refer correspondingly to planar and relaxed configurations of the porphyrin ring.

TABLE 1: Distance Dependence of Electron-Transfer Coupling Energies (V_{RP}), in Wavenumbers, as a Function of Iron Separation for Model Heme Dimers[a]

heme dimer	$V_{RP}(r) = V^0_{RP} \exp(-\beta r/2)$	
	V^0_{RP} ($r = 16.5$)	β
A	1.6	2.0
B	8.0	2.6
C	6.6	2.2
D	540	4.0
E	0.2	1.1

[a] The decay parameter β is in Å^{-1}. The reference value V^0_{RP} is taken at r_{Fe-Fe} = 16.5 Å, and the iron−iron distance is relative to that separation.

TABLE 2: Electron-Transfer Coupling Energies (V_{RP}) in Wavenumbers and Electronic Transmission Coefficients κ (in Parentheses) of Ifc_3 Model Heme Dimers

heme dimer	Fe−Fe distance (Å)	edge−edge distance (Å)	V_{RP} (κ)
HEC801 HEC802	12.4	5.6	73 (0.14)
HEC802 HEC803	10.0	3.9	286 (0.84)
HEC803 HEC804	15.7	6.5	1 (2.7×10^{-5})

dimers. According to eqs 56a and 56b in ref 30, the electronic coupling should decay with increased iron−iron separation according to $V_{RP} = V^0_{RP} \exp(-\beta r/2)$. The linear plots of $\ln(V_{RP})$ versus the iron−iron separation r_{Fe-Fe} between the hemes in Figure 6 show that all five dimers obey exponential dependence, in which the slope of each line is $-\beta/2$.

Since κ is most sensitive to V_{RP}, $\log(\kappa)$ also decays linearly with increased iron−iron separation (Figure 7). The point at which the $\log(\kappa)$ versus r_{Fe-Fe} curve crosses the x-axis corresponds $\log(\kappa) = 0$ or $\kappa = 100\%$. By extrapolation of each line to that point, the perfectly adiabatic heme separation can be estimated.

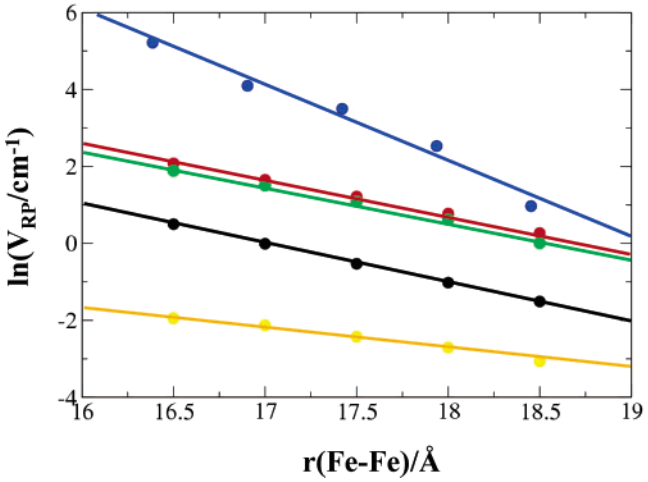

Figure 6. Distance dependence of heme dimer electronic coupling, $\ln(V_{RP})$ vs iron−iron separation. The slope of each line is $-\beta/2$. The reference value V^0_{RP} is taken at r_{Fe-Fe} = 16.5 Å, and the iron−iron distance is relative to that separation. The colors correspond to the dimers shown in Figure 4. Dimer A is black, B is red, C is green, D is blue, and E is yellow.

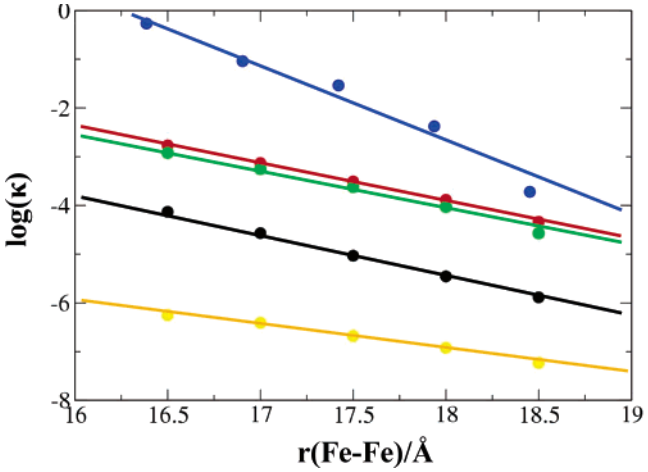

Figure 7. Distance dependence of heme dimer Landau−Zener electron hopping probabilities. The x-intercept is the iron separation which is 100% adiabatic ($\kappa = 1.0$). The colors correspond to the dimers shown in Figure 4. Dimer A is black, B is red, C is green, D is blue, and E is yellow.

For dimer A, $\kappa = 100\%$ when r_{Fe-Fe} = 11.8 Å, at which point the imidazole hydrogens are in van der Waals contact and V_{RP} is 217 cm^{-1} (by extrapolating V_{RP} vs r_{Fe-Fe}). In the parallel heme dimers B and C, there is only a slight difference between their respective electronic coupling and hopping probabilities. The coplanar arrangement of the imidazoles in dimer B increases the overlap very slightly, and both dimers have an adiabatic r_{Fe-Fe} separation of 13.0 Å, which is a separation of 4.0 Å between the porphyrins of each monomer. At this separation, V_{RP} is 193 and 186 cm^{-1} for dimers B and C, respectively.

The dimers with perpendicular porphyrin planes show how dramatically the orientation of the hemes affects their electronic coupling and decay parameters. In dimer D, the hemes are rotated and staggered so that the porphyrin edges meet at a 90° angle. In this dimer, the decay parameter β is the largest. However, when the hemes are aligned so that the first heme's porphyrin plane aligns with the second heme's iron (dimer E),

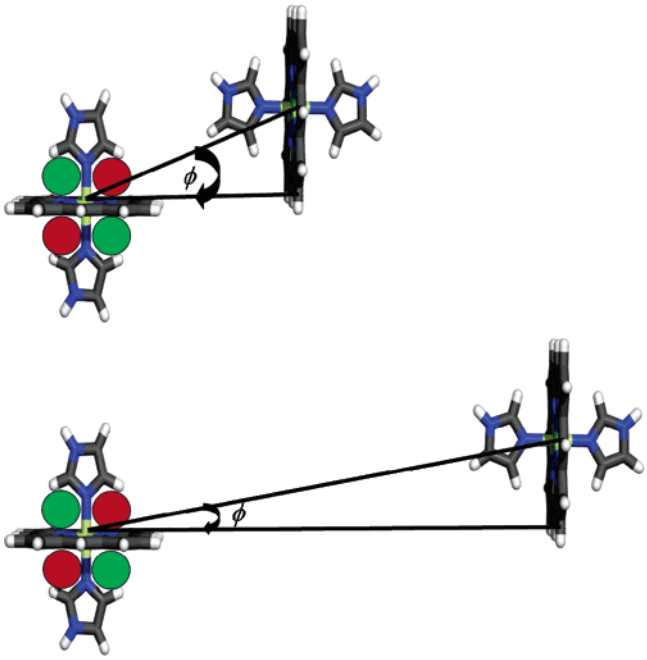

Figure 8. The amount of d_π nodal character in the angle ϕ subtended by one heme iron at the other increases with increased heme separation, yielding its large exponential decay constant. For clarity, the lobes of the Fe(d_π) orbital on the first heme are represented by red and green circles.

the decay parameter is the smallest. Siders, Cave, and Marcus calculated electronic coupling elements and their decay with distance using a single-particle Schrödinger equation.[37,38] Mirroring their analysis of the orientation effect on the decay constant, if ϕ, the angle subtended by one heme iron at the other, includes more and more of the node of one heme iron's d_π orbital as the dimer separation increases, then a large decay constant will result. Figure 8 shows that this is indeed the case with heme dimer D.

The distance dependence results for the model dimers A−E help interpret the electronic coupling data for the hemes in the orientation observed in Ifc_3 and similar tetraheme proteins. The first electron-transfer step moves an electron between HEC801 (closest to the cytoplasmic membrane of *S. frigidimarina*) to HEC802, its nearest neighboring heme. κ is 0.14, so 14% of excitations to the crossing-point configuration will lead to electron transfer. The orientation of the porphyrin planes is semiperpendicular, and only a small rotation is needed to achieve the optimal configuration of model dimer D above. Electron transfer between HEC802 and HEC803 is very easy, and 84% of excitations to the crossing-point configuration will lead to electron transfer. HEC802 and HEC803 are closest together, and the porphyrin planes are stacked, so the decay parameter $\beta \approx 2$ Å^{-1}. The ET step from HEC803 to HEC804 has the largest iron−iron distance, and their orientation is similar to dimer E, which has the smallest coupling and the strongest distance dependence. All of these factors make this the rate-limiting step in the overall electron transfer, but again rotating one of the hemes would make it adiabatic. HEC801 and HEC804 are near the surface of the enzyme, HEC802 is partially exposed, and HEC803 is bound by the protein matrix. Therefore, the rate-limiting third ET step is controlled by both protein and solvent dynamics at the enzyme surface, which control the donor−acceptor distance and the angle between heme planes.

Summary and Future Directions

We have shown that the conserved relative heme orientation in Ifc_3, Fcc_3, and others gives the protein an added measure of control over the long-range electron transfer. By controlling not only the distance between redox centers but also the orientation, the protein can tune the overlap between donor and acceptor orbitals and facilitate ET at each stage of the reaction. We have also shown that the imidazole planes can rotate freely, so the histidine plane orientations observed experimentally are constrained by the residues attached to the histidines.

The B3LYP results presented here quantify the contributions of the first coordination sphere on the redox properties of heme proteins. Future investigations should account for the heterogeneous protein environment because ET rates in cytochromes are often thought to be limited by the effective frequency of fluctuations in the protein and/or the solvent, the so-called relaxation-limited case.[39] It is also important to recognize that other protein residues can participate directly as bridge groups in the ET.[35,40] In a survey of electron-transfer proteins, it was shown that electrons can travel up to 14 Å between redox centers[41] and ET over longer distances (such as the 16 Å distance between HEC803 and HEC804) involves bridging groups.

Acknowledgment. This work was supported in part by the Office of Advanced Scientific Computing Research, Office of Science, U. S. Department of Energy, and also by the Engineering and Geosciences Division of the Office of Basic Energy Sciences, U. S. Department of Energy. D.M.A.S. thanks Dr. Erich Vorpagel for very helpful discussions and Dr. Wlodek Apostoluk for preparing Figure 1. Computational resources for this work were provided by the Molecular Sciences Computing Facility of the Environmental Molecular Sciences Laboratory at Pacific Northwest National Laboratory. Pacific Northwest National Laboratory is operated for the U. S. Department of Energy by the Battelle Memorial Institute.

References and Notes

(1) Lloyd, J. R.; Chesnes, J.; Glasauer, S.; Bunker, D. J.; Livens, F. R.; Lovley, D. R. *Geomicrobiol. J.* **2002**, *19*, 103.
(2) Lovley, D. R. *Annu. Rev. Microbiol.* **1993**, *47*, 263.
(3) Bowman, J. P.; McCammon, S. A.; Nichols, D. S.; Skerratt, J. H.; Rea, S. M.; Nichols, P. D.; McMeekin, T. A. *Int. J. Syst. Bacteriol.* **1997**, *47*, 1040.
(4) Leys, D.; Meyer, T. E.; Tsapin, A. S.; Nealson, K. H.; Cusanovich, M. A.; Van Beeumen, J. J. *J. Biol. Chem.* **2002**, *277*, 35703.
(5) Baik, M. H.; Crystal, J. B.; Friesner, R. A. *Inorg. Chem.* **2002**, *41*, 5926.
(6) Smith, D. M. A.; Dupuis, M.; Straatsma, T. P. *Mol. Phys.* **2004**, *103*, 273.
(7) Smith, D. M. A.; Dupuis, M.; Vorpagel, E. R.; Straatsma, T. P. *J. Am. Chem. Soc.* **2003**, *125*, 2711.
(8) Godbout, N.; Havlin, R.; Salzmann, R.; Debrunner, P. G.; Oldfield, E. *J. Phys. Chem. A* **1998**, *102*, 2342.
(9) Godbout, N.; Sanders, L. K.; Salzmann, R.; Havlin, R. H.; Wojdelski, M.; Oldfield, E. *J. Am. Chem. Soc.* **1999**, *121*, 3829.
(10) Kuramochi, H.; Noodleman, L.; Case, D. A. *J. Am. Chem. Soc.* **1997**, *119*, 11442.
(11) Grodzicki, M.; Flint, H.; Winkler, H.; Walker, F. A.; Trautwein, A. X. *J. Phys. Chem. A* **1997**, *101*, 4202.
(12) Zhang, Y.; Mao, J. H.; Godbout, N.; Oldfield, E. *J. Am. Chem. Soc.* **2002**, *124*, 13921.
(13) Zhang, Y.; Mao, J. H.; Oldfield, E. *J. Am. Chem. Soc.* **2002**, *124*, 7829.
(14) Kozlowski, P. M.; Spiro, T. G.; Zgierski, M. Z. *J. Phys. Chem. B* **2000**, *104*, 10659.
(15) Spiro, T. G.; Zgierski, M. Z.; Kozlowski, P. M. *Coord. Chem. Rev.* **2001**, *219*, 923.
(16) Sato, F.; Yoshihiro, T.; Era, M.; Kashiwagi, H. *Chem. Phys. Lett.* **2001**, *341*, 645.

(17) Loew, G. H.; Harris, D. L. *Chem. Rev.* **2000**, *100*, 407.
(18) Johansson, M. P.; Blomberg, M. R. A.; Sundholm, D.; Wilkstron, M. *Biochim. Biophys. Acta* **2002**, *1553*, 183.
(19) Johansson, M. P.; Sundholm, D.; Gerfen, G.; Wikstrom, M. *J. Am. Chem. Soc.* **2002**, *124*, 11771.
(20) Scherlis, D. A.; Estrin, D. A. *Int. J. Quantum Chem.* **2002**, *87*, 158.
(21) Du, P.; Loew, G. H. *J. Am. Chem. Soc.* **1991**, *95*.
(22) Oganesyan, V. S.; Sharonov, Y. A. *Spectrochim. Acta, Part A* **1997**, *53*, 433.
(23) Walker, F. A. *Coord. Chem. Rev.* **1999**, *186*, 471.
(24) Field, S. J.; Dobbin, P. S.; Cheesman, M. R.; Watmough, N. J.; Thomson, A. J.; Richardson, D. J. *J. Biol. Chem.* **2000**, *275*, 8515.
(25) Marcus, R. A. *Annu. Rev. Phys. Chem.* **1964**, *15*, 155.
(26) Marcus, R. A. *J. Chem. Phys.* **1956**, *26*, 966.
(27) Zener, C. *Proc. R. Soc. London, Ser. A* **1932**, *137*, 696.
(28) Landau, L. *Phys. Z. Sowjetunion* **1932**, *89*, 1.
(29) Marcus, R. A.; Sutin, N. *Biochim. Biophys. Acta* **1985**, *35*, 437.
(30) Newton, M. D.; Sutin, N. *Annu. Rev. Phys. Chem.* **1984**, *35*, 437.
(31) Nelsen, S. F.; Blackstock, S. C.; Kim, Y. *J. Am. Chem. Soc.* **1987**, *109*, 677.
(32) Rosso, K. M.; Rustad, J. R. *J. Phys. Chem. A* **2000**, *104*, 6718.
(33) Klimkans A.; S., L. *Chem. Phys.* **1994**, *189*, 25.
(34) Rosso, K. M.; Smith, D. M. A.; Dupuis, M. *J. Chem. Phys.* **2003**, *118*, 6455.
(35) Simonson, T. *Rep. Prog. Phys.* **2003**, *66*, 737.
(36) Harrison, R. J.; Nichols, J. A.; Straatsma, T. P.; Dupuis, M.; Bylaska, E. J.; Fann, G. I.; Windus, T. L.; Apra, E.; de Jong, W.; Hirata, S.; Hackler, M. T.; Anchell, J.; Bernholdt, D.; Borowski, P.; Clark, T.; Clerc, D.; Dachsel, H.; Deegan, M.; Dyall, K.; Elwood, D.; Fruchtl, H.; Glendening, E.; Gutowski, M.; Hirao, K.; Hess, A.; Jaffe, J.; Johnson, B.; Ju, J.; Kendall, R.; Kobayashi, R.; Kutteh, R.; Lin, Z.; Littlefield, R.; Long, X.; Meng, B.; Nakajima, T.; Nieplocha, J.; Niu, S.; Rosing, M.; Sandrone, G.; Stave, S.; Taylor, H.; Thomas, G.; van Lenthe, J.; Wolinski, K.; Wong, A.; Zhang, Z. *NWChem, A Computational Chemistry Package for Parallel Computers*, version 4.1; 2002.
(37) Siders, P.; Cave, R. J.; Marcus, R. A. *J. Chem. Phys.* **1984**, *81*, 5613.
(38) Cave, R. J.; Siders, P.; Marcus, R. A. *J. Phys. Chem.* **1986**, *90*, 1436.
(39) Cherepanov, D. A.; Krishtalik, L. I.; Mulkidjanian, A. Y. *Biophys. J.* **2001**, *80*, 1033.
(40) Jeuken, L. J. C.; Jones, A. K.; Chapman, S. K.; Cecchini, G.; Armstrong, F. A. *J. Am. Chem. Soc.* **2002**, *124*, 5702.
(41) Page, C. C.; Moser, C. C.; Chen, X. X.; Dutton, P. L. *Nature* **1999**, *402*, 47.